Proc. of SPIE Vol. 0748, Structural Mechanics of Optical Systems II, ed. A.E. Hatheway (Jan 1987) Copyright SPIE

Response of large optical mirrors to thermal distributions

E. Pearson and L. Stepp

Advanced Development Program, National Optical Astronomy Observatories*
P. O. Box 26732, Tucson, Arizona 85726-6732

Abstract

The National New Technology Telescope program at NOAO is developing technology to be used in the design of a 15-meter multiple-mirror telescope. One configuration being considered for the primary mirrors is a lightweight honeycomb sandwich structure cast from borosilicate glass. This material has a relatively large coefficient of thermal expansion (about 3 parts per million per degree C) which can produce optically-significant distortions when the mirror is exposed to a typical observatory thermal environment. To study this problem we have tested a prototype borosilicate glass mirror, 1.8 meters in diameter, in various thermal environments.

Finite-element modeling was used to predict the thermal distortions of the optical surface. This led to an analysis in which temperature patterns were described by a least-squares fit to a polynomial expression, and the polynomial was then used to predict nodal temperatures of the model. The individual terms of the polynomial describe patterns of temperature such as linear-diametral gradients, radial gradients, etc. The optical distortions resulting from these cases are described in this paper. An analytical solution for a 3-dimensional linear temperature gradient was developed to check the finite-element results, and is also presented.

Introduction

The National New Technology Telescope (NNTT) will be a 15-meter multiple mirror telescope with four 7.5-meter primary mirrors. A conceptual model of the telescope is shown in Figure 1.

The use of lightweight primary mirrors is expected to reduce the overall mass, thermal inertia, and cost of the telescope. One promising type of lightweight mirror blank is a cast borosilicate glass honeycomb-core sandwich panel (see Figure 2). With funding from the NNTT program, the University of Arizona is developing the capability to cast lightweight borosilicate mirror blanks up to 8 meters in diameter. Three successful 1.8-meter blanks have been cast, and preparations are under way to cast a 3.5-meter blank.

The primary disadvantage of this type of mirror blank is the relatively high coefficient of thermal expansion of borosilicate glass - approximately 3 parts per million per degree C. The image quality goals for the NNTT are to produce images of 1/4 arcsecond (full-width-half-maximum). Thermal distortion of the primary mirrors is being investigated to ensure the telescope will be able to meet these goals.

This past year, a study was conducted using one of the 1.8-meter blanks to investigate distortion of the mirror from thermal effects[1]. Temperatures were measured at 57 locations on the mirror structure, and the optical surface figure was measured with a scatterplate interferometer. There was no simple correlation between the temperature variations measured and the mirror distortion which resulted, but it was obvious that the magnitude of distortion was appreciable even for temperature variations of less than a degree C.

Because we were not able to predict the thermal distortion reliably using such a simple measure as overall temperature range in the mirror, we extended the analysis to take into account the pattern of temperature distribution. A number of finite element models were constructed, but preparing thermal data for such models is difficult. Either the nodal temperatures or the element temperatures (or both) have to be known. A model of a structured mirror requires a large number of nodes and elements, and measurement of the temperatures is difficult in practice. In a material with low thermal conductivity, measurement of the temperatures at the surface is not guaranteed to provide accurate information about internal temperatures. Also, the number of nodes or elements is normally greater than the number of thermal sensors that can be practically located on the mirror. For these reasons it is necessary to extrapolate from measured data to predict the

*Operated by the Association of Universities for Research in Astronomy, Inc., under contract with the National Science Foundation.

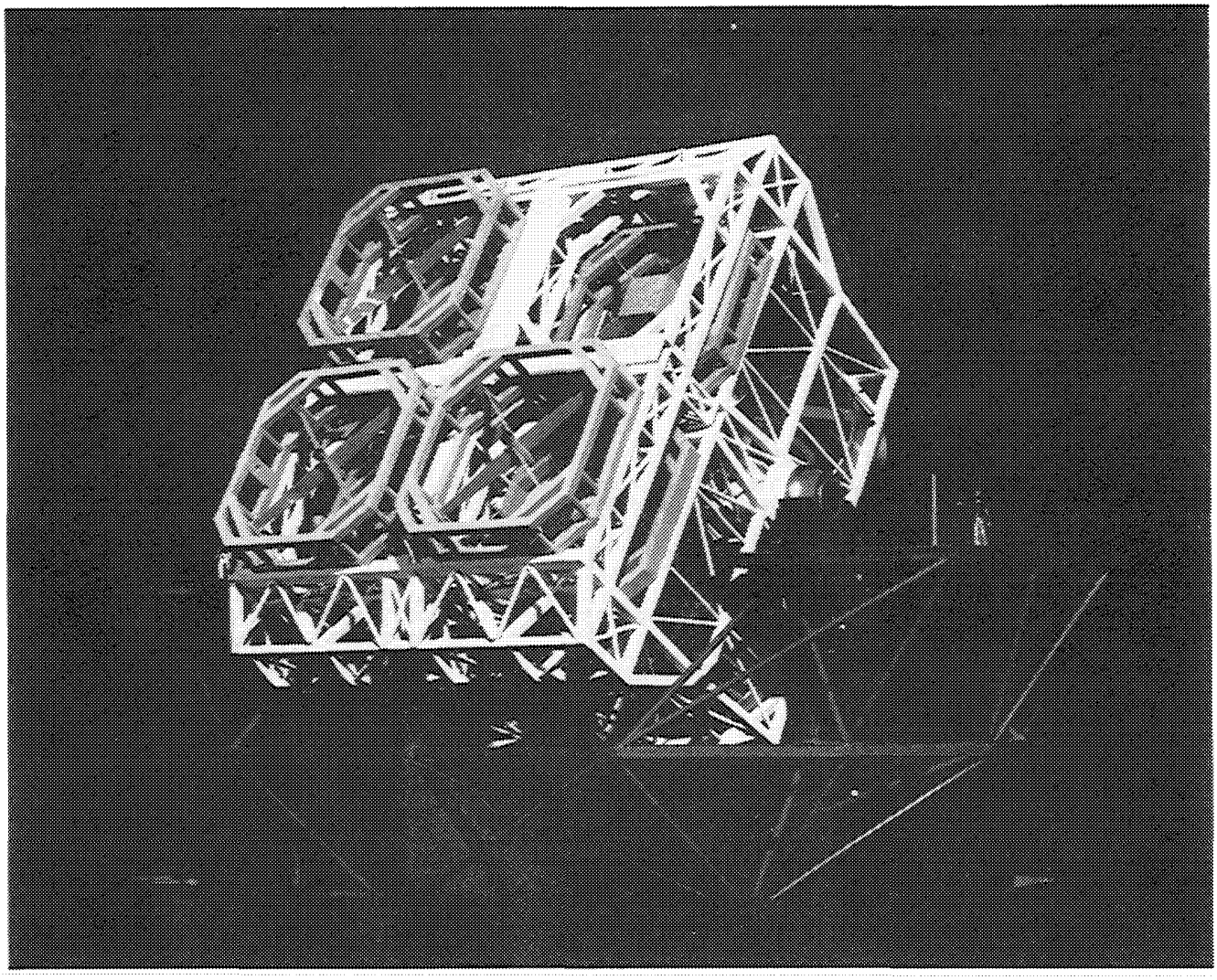

Figure 1. A conceptual model of the National New Technology Telescope, a multiple mirror telescope with four 7.5-meter mirrors.

temperatures that occur at each node or element. The 57 thermistors used in the experiment were divided into three groups: (a) underneath the upper (mirror) surface, (b) on the ribs at the midplane, and (c) along the back surface. The finite-element models were constructed with nodes at three levels corresponding to the thermistor location levels. In order to predict the nodal temperatures from the measured values, the temperatures at each level were fit to a polynomial:

$$T(x,y) = K_1 + K_2(x) + K_3(y) + K_4(2x^2 + 2y^2 - 1) + K_5(x^2 - y^2) + K_6(2xy) + K_7(3x^3 + 3xy^2 - 2x) + K_8(3x^2y + 3y^3 - 2y) + K_9(6x^4 + 12X^2y^2 + 6y^4 - 6x^2 - 6y^2 + 1) \quad (1)$$

This polynomial consists of 9 terms of the Zernike series, expressed in rectangular Cartesian coordinates. The origin is at the center of the mirror surface with the z-axis along the optical axis and x and y have been normalized over the mirror half-diameter. Using a least-squares fit, the 9 coefficients for each level are obtained and can be used to predict the temperature at each nodal position. The accuracy of this method was limited by the uncertainty of using surface measurements to characterize internal glass temperatures and by the relatively sparse number of data points at each level. In spite of these limitations, the general agreement between the measured optical surface and the distortion

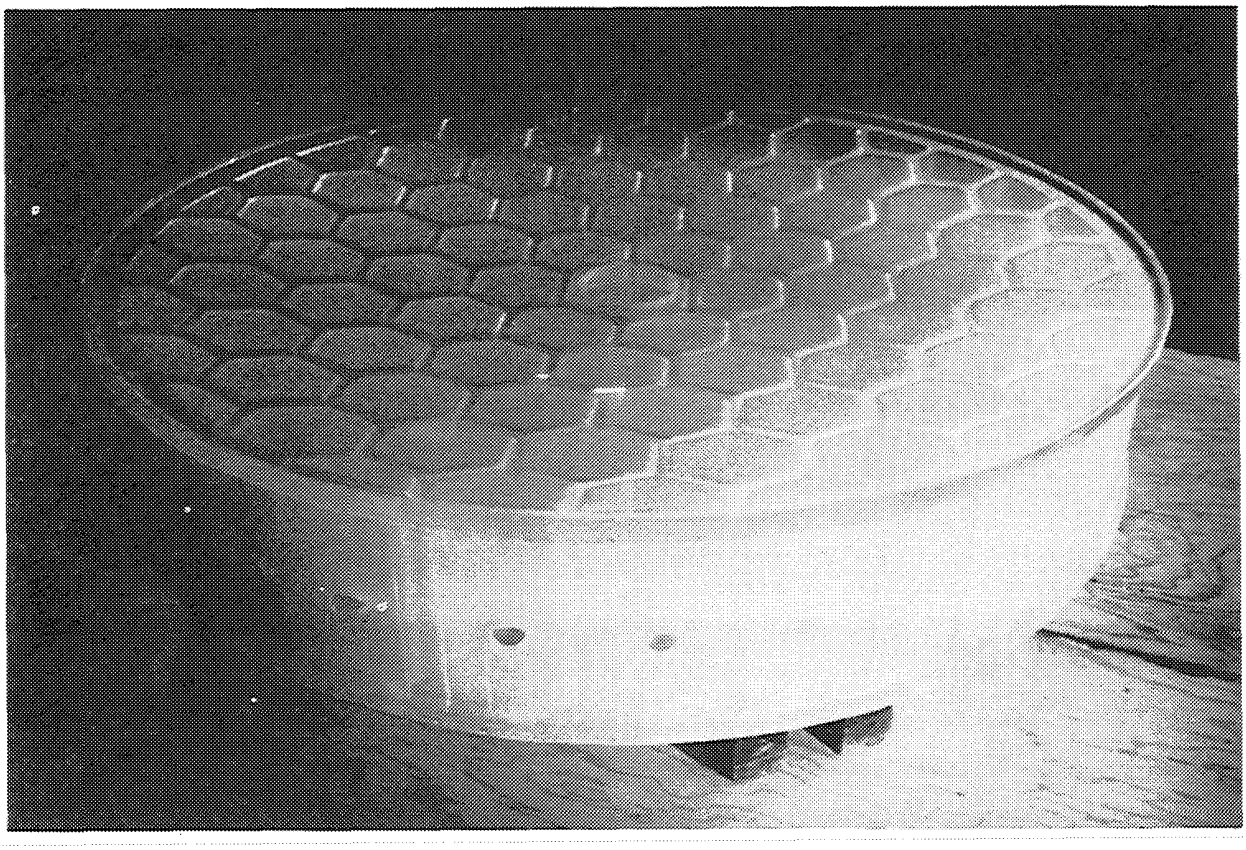

Figure 2. A 1.8-meter diameter lightweight mirror cast from borosilicate glass by the Steward Mirror Lab at the University of Arizona, under contract to the National Optical Astronomy Observatories. Photo courtesy Steward Observatory, University of Arizona.

predicted by the finite element model was encouraging[1]. As an extension of that work, we have explored the effect of different temperature patterns by applying one term of the polynomial at a time to the finite element model, which is the subject of this paper.

Description of the finite-element model

The structural program used for this study was SAP IV[2]. To obtain the best thermo-elastic results, plane stress elements were used. These use nodal temperatures with linear interpolation between nodes. (This model was different than the structural model we used to study the effects of support forces, which used plate bending elements.) Although previous models had been constructed with three levels of nodes, it was found that a thermal pattern applied to the midplane had a significantly smaller effect than the same pattern applied to the front or back surface. Therefore, the model used for this study had only two levels of nodes.

A pre-processor program was written to prepare the SAP IV data files; each nodal temperature was calculated using the coordinates of the node and the expression for the polynomial term being modeled. This allowed rapid data preparation for a sequence of different analysis runs.

To check the accuracy of the results from the model, an analytical solution was derived for a mirror with a parabolic surface subjected to the thermal distribution:

$$T(x,y,z) = C_0 + C_1(x) + C_2(y) + C_3(z) \qquad (2)$$

where C_0, C_1, C_2 and C_3 are constants. The resulting deformations can be grouped into aberration terms, as follows:

$$\begin{aligned} W(r,\theta) = {} & (\alpha C_3/8R^2)r^4 && \text{(spherical)} \\ & +(\alpha C_1/2R)r^3\cos(\theta) + (\alpha C_2/2R)r^3\sin(\theta) && \text{(coma)} \\ & + (\alpha C_3 Z_0/2R - \alpha C_3/2 + \alpha C_0/2R)r^2 && \text{(focus)} \\ & + (\alpha C_1 Z_0 - C_4)r\cos(\theta) + (\alpha C_2 Z_0 - C_5)r\sin(\theta) && \text{(tilt)} \\ & + (\alpha C_3 Z_0^2/2 + \alpha C_0 Z_0 - C_6) && \text{(piston)} \end{aligned} \qquad (3)$$

Where:

- W = mirror surface deformation caused by temperature
- r = radius position on surface ($r = \sqrt{x^2+y^2}$)
- θ = angular position on surface (θ = arctan(y/x))
- α = coefficient of thermal expansion
- R = paraxial radius of curvature
- Z_0 = axial thickness of mirror
- C_4, C_5, C_6 = arbitrary tilts and piston that depend on the mirror defining system.

To verify the accuracy of the model for our study, we analyzed several cases of this type. The agreement between the finite element model and the exact solution was always within 1%. The effects of gravity are not included in this analysis. Any combination of thermal distortion and gravity effects can be found by superimposing individual thermal cases with gravity loading cases run earlier.

Some insights can be gained from looking at the results of the individual thermal cases. Eighteen analysis runs were made, applying a unit value to each of the 9 terms in the polynomial expansion in succession, one surface at a time. These are shown in Figures 3 through 20, and summarized in Table 1.

The linear temperature interpolation between nodes of the plane stress elements can represent exactly the first three terms in equation 1, and closely approximates the other 6 terms. The plots of thermal patterns reproduced in Figures 3 through 20 were constructed to illustrate this approximation, and some deviation from smooth curves can be seen for the higher order terms. If additional terms of the Zernike series were included in equation 1, more elements should be used to improve the fit to the higher order terms.

The optical surface plots for this paper were produced using the WISP program*, which requires the surface information in each case to be approximated by a 36-term Zernike polynomial. In general this approach introduces errors into the data, however, because of the smooth nature of the thermal input the largest error in these cases is less than 1/10 wave peak-to-valley.

Results

In each figure, the first pattern shows the thermal input superimposed on the pattern of elements, and the second and third show the distortion of the optical surface after focus and tilt corrections have been made. Figures 3 through 11 show the distortion resulting from a thermal pattern applied to the front surface of the mirror, and Figures 12 through 20 show the optical surface distortion from patterns applied to the back surface. In each case the coefficient is given a unit value, so the temperature pattern has a maximum value of 1°C.

*(Wyant Interferogram Software Program), WYKO Corporation, Tucson, Arizona

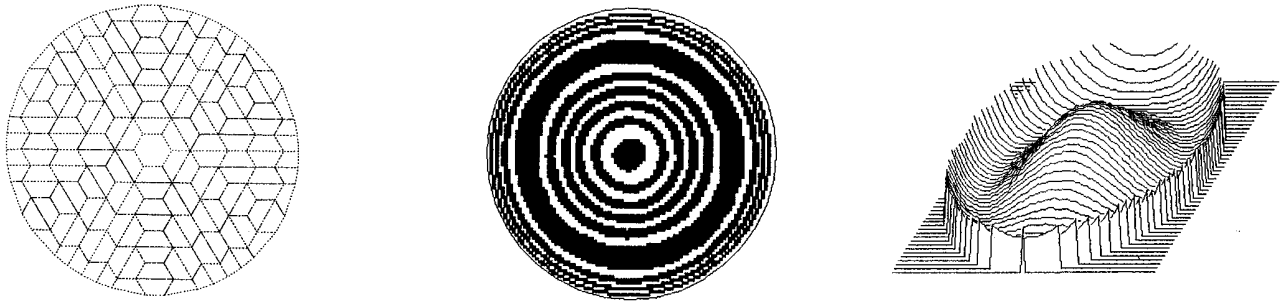

Temperature pattern
(uniform)

Optical surface
contour interval:0.01λ P-V:0.05λ RMS:0.01λ

Figure 3. Distortion caused by temperature pattern T = 1°C on front surface, T = 0°C on back surface.

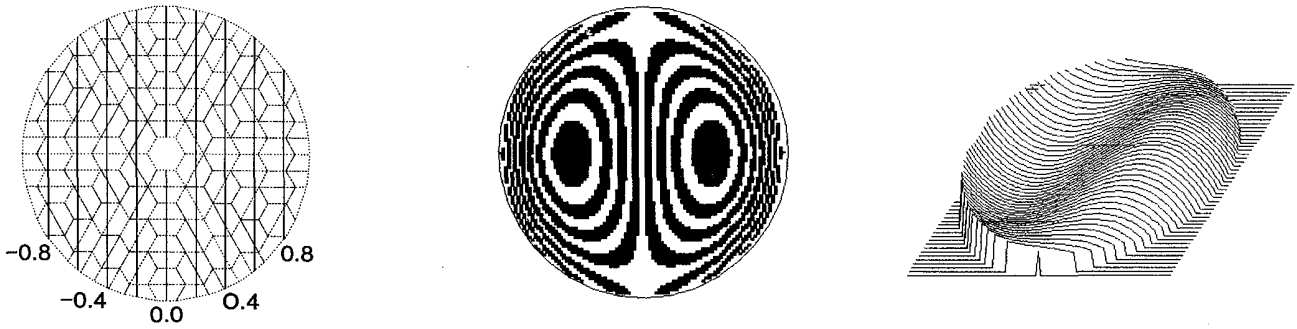

Temperature pattern
(front surface)

Optical surface
contour interval:0.25λ P-V:1.84λ RMS 0.45λ

Figure 4. Distortion caused by temperature pattern T = (1°C)(x) on front surface, T = 0°C on back surface. Note the change of scale.

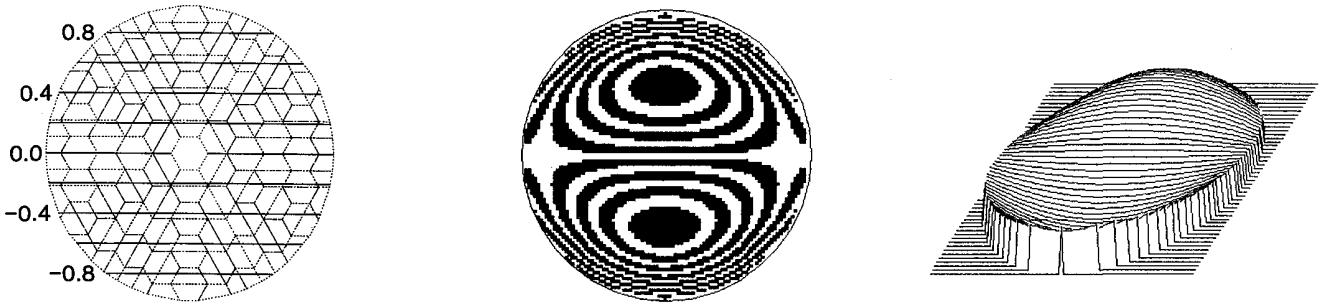

Temperature pattern
(front surface)

Optical surface
contour interval:0.25λ P-V:1.81λ RMS 0.44λ

Figure 5. Distortion caused by temperature pattern T = (1°C)(y) on front surface, T = 0°C on back surface.

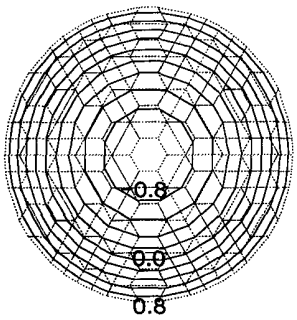

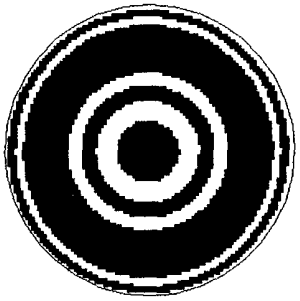

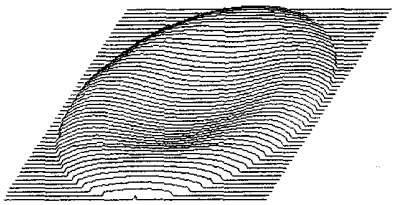

Temperature pattern
(front surface)

Optical surface
contour interval:0.25λ P-V:0.52λ RMS 0.14λ

Figure 6. Distortion caused by temperature pattern T = (1°C)($2x^2 + 2y^2 - 1$) on front surface, T = 0°C on back surface.

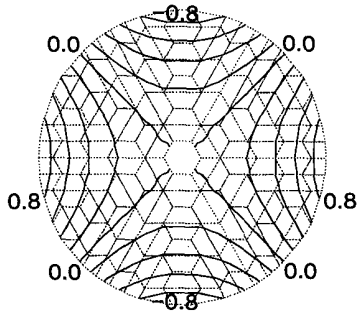

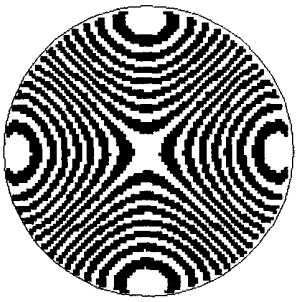

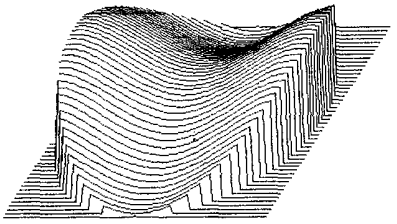

Temperature pattern
(front surface)

Optical surface
contour interval:0.25λ P-V:3.48λ RMS 0.96λ

Figure 7. Distortion caused by temperature pattern T = (1°C)($x^2 - y^2$) on front surface, T = 0°C on back surface.

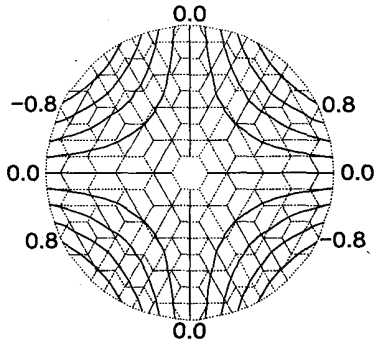

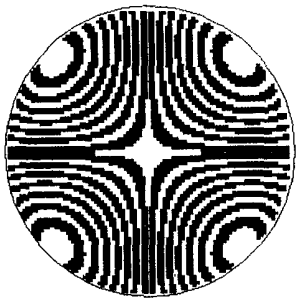

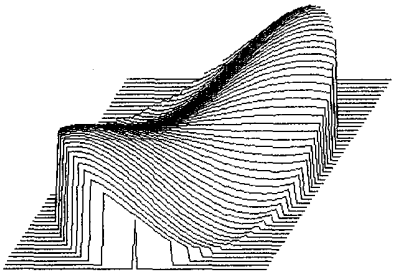

Temperature pattern
(front surface)

Optical surface
contour interval:0.25λ P-V:3.55λ RMS 0.95λ

Figure 8. Distortion caused by temperature pattern T = (1°C)(2xy) on front surface, T = 0°C on back surface.

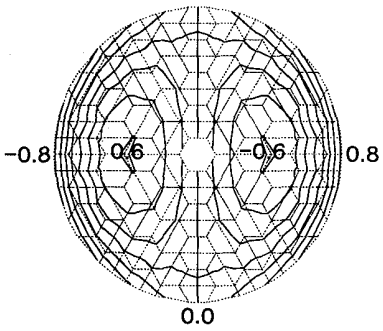

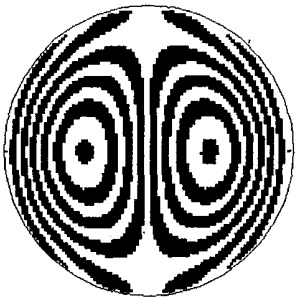

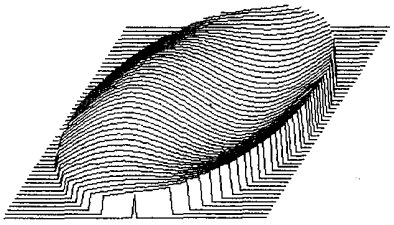

Temperature pattern (front surface)

Optical surface
contour interval:0.25λ P-V:1.62λ RMS 0.37λ

Figure 9. Distortion caused by temperature pattern T = (1°C)($3x^3 + 3xy^2 - 2x$) on front surface, T = 0°C on back surface.

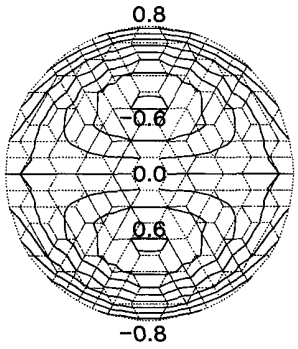

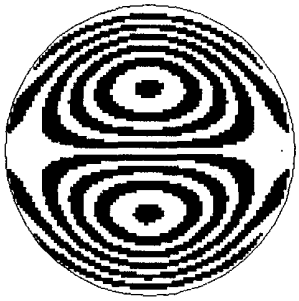

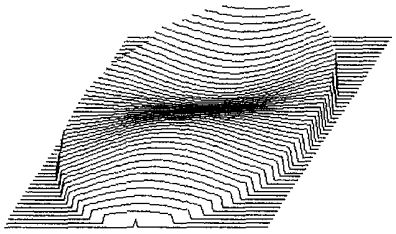

Temperature pattern (front surface)

Optical surface
contour interval:0.25λ P-V:1.61λ RMS 0.36λ

Figure 10. Distortion caused by temperature pattern T = (1°C)($3x^2y + 3y^3 - 2y$) on front surface, T = 0°C on back surface.

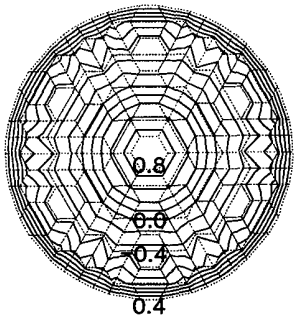

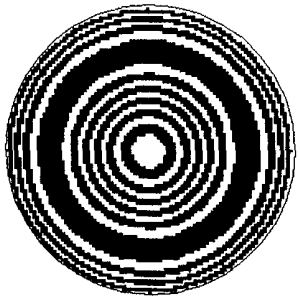

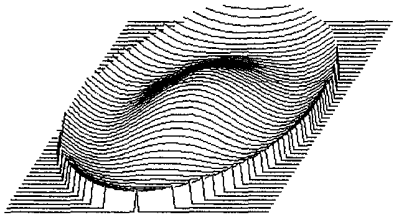

Temperature pattern (front surface)

Optical surface
contour interval:0.25λ P-V:1.32λ RMS 0.31λ

Figure 11. Distortion caused by temperature pattern T = (1°C)($6x^4+12x^2y^2+6y^4-6x^2-6y^2+1$) on front surface, T = 0°C on back surface.

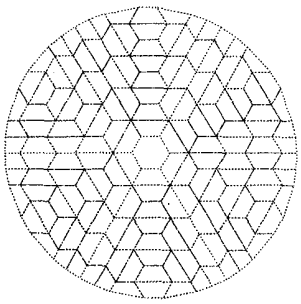

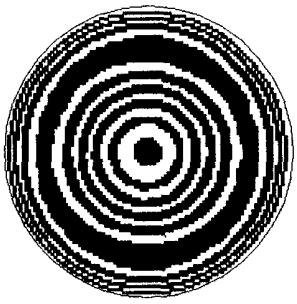

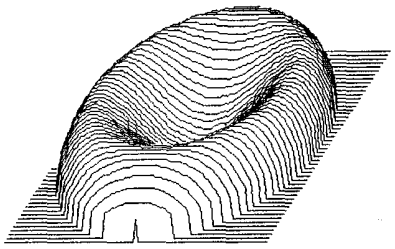

Temperature pattern
(front surface)

Optical surface
contour interval:0.01λ P-V:0.05λ RMS 0.01λ

Figure 12. Distortion caused by temperature pattern T = 0°C on front surface, T = 1°C on back surface. Note the change of scale.

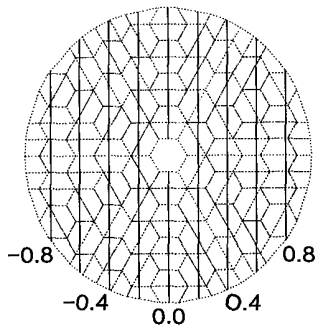

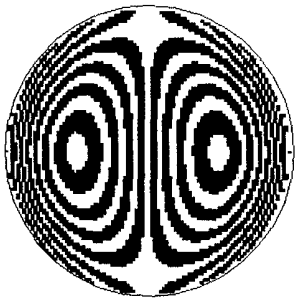

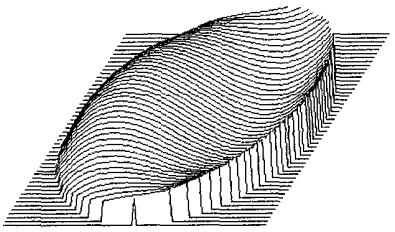

Temperature pattern
(uniform)

Optical surface
contour interval:0.25λ P-V:1.95λ RMS 0.47λ

Figure 13. Distortion caused by temperature pattern T = 0°C on front surface, T = (1°C)(x) on back surface. Note the change of scale.

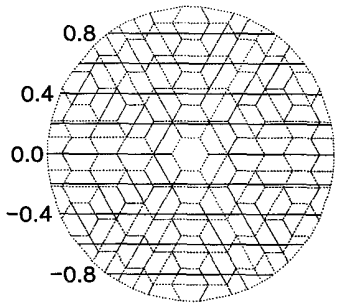

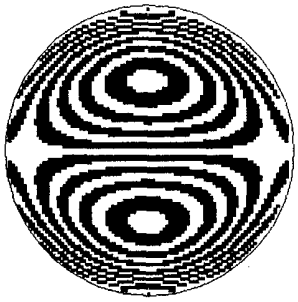

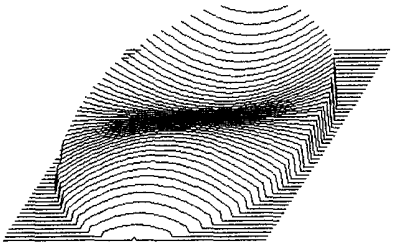

Temperature pattern
(back surface)

Optical surface
contour interval:0.25λ P-V:1.92λ RMS 0.47λ

Figure 14. Distortion caused by temperature pattern T = 0°C on front surface, T = (1°C)(y) on back surface. Note the change of scale.

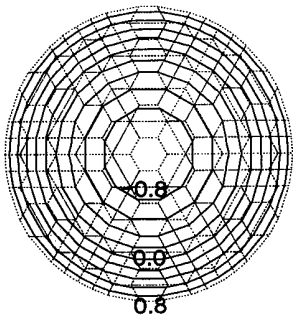

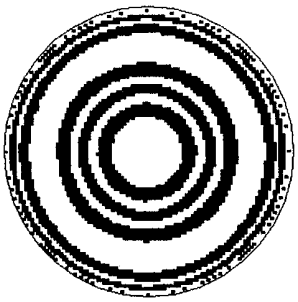

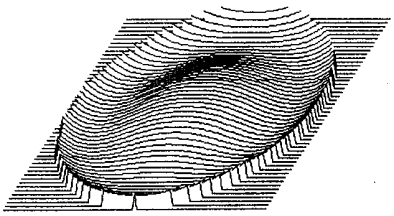

Temperature pattern
(back surface)

Optical surface
contour interval:0.25λ P-V:0.79λ RMS 0.21λ

Figure 15. Distortion caused by temperature pattern T = 0°C on front surface, T = (1°C)($2x^2 + 2y^2 - 1$) on back surface.

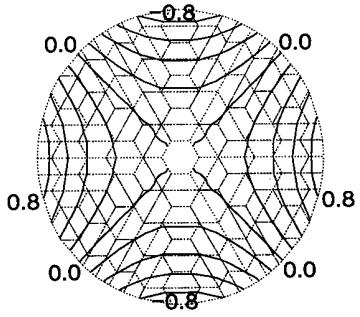

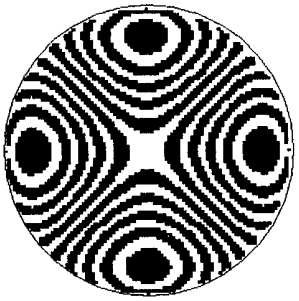

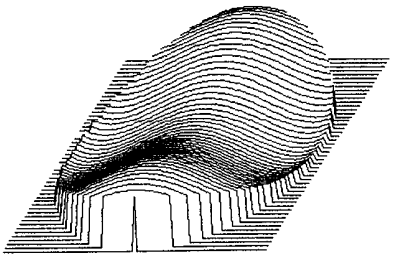

Temperature pattern
(back surface)

Optical surface
contour interval:0.25λ P-V:2.26λ RMS 0.64λ

Figure 16. Distortion caused by temperature pattern T = 0°C on front surface, T = (1°C)($x^2 - y^2$) on back surface.

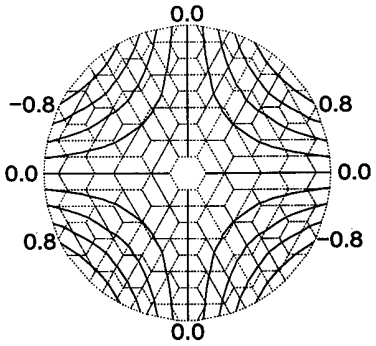

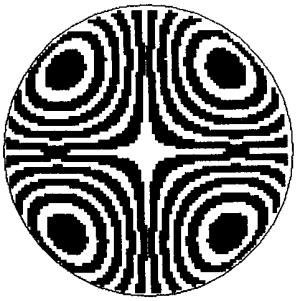

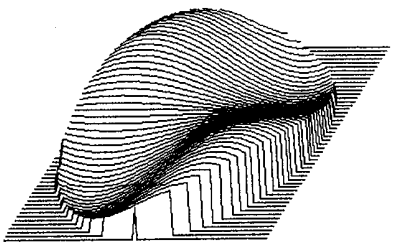

Temperature pattern
(back surface)

Optical surface
contour interval:0.25λ P-V:2.24λ RMS 0.63λ

Figure 17. Distortion caused by temperature pattern T = 0°C on front surface, T = (1°C)(2xy) on back surface.

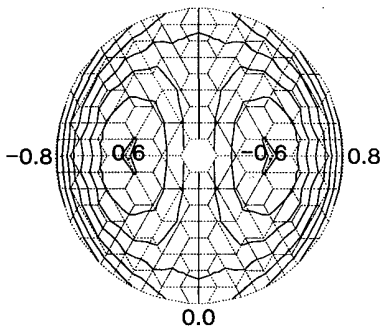

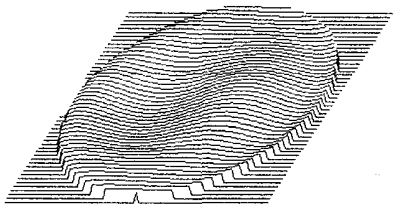

Temperature pattern (back surface)

Optical surface
contour interval:0.25λ P-V:0.67λ RMS 0.13λ

Figure 18. Distortion caused by temperature pattern T = 0°C on front surface, $T \doteq (1^{\circ}C)(3x^3 + 3xy^2 - 2x)$ on back surface.

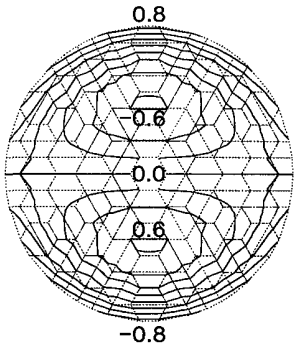

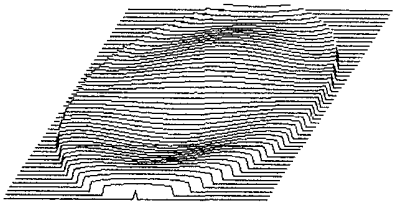

Temperature pattern (back surface)

Optical surface
contour interval:0.25λ P-V:0.69λ RMS 0.12λ

Figure 19. Distortion caused by temperature pattern T = 0°C on front surface, $T = (1^{\circ}C)(3x^2y + 3y^3 - 2y)$ on back surface

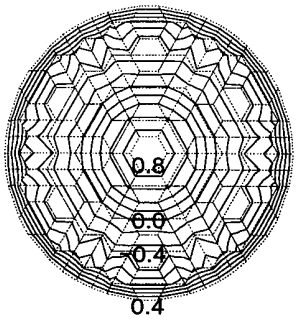

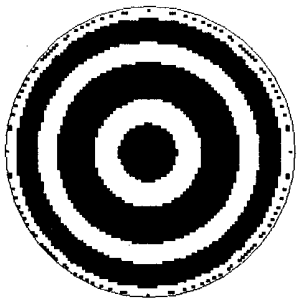

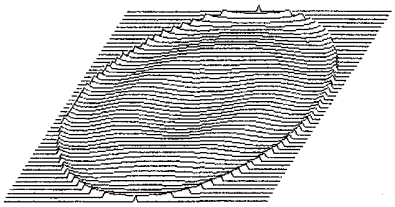

Temperature pattern (back surface)

Optical surface
contour interval:0.25λ P-V:0.22λ RMS 0.06λ

Figure 20. Distortion caused by temperature pattern T = 0°C on front surface, $T = (1^{\circ}C)(6x^4 + 12x^2y^2 + 6y^4 - 6x^2 - 6y^2 + 1)$ on back surface.

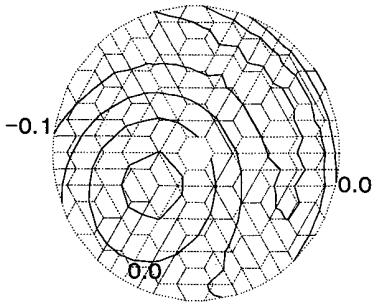

Temperature pattern
(front surface)

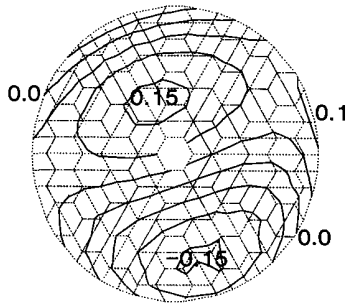

Temperature pattern
(back surface)

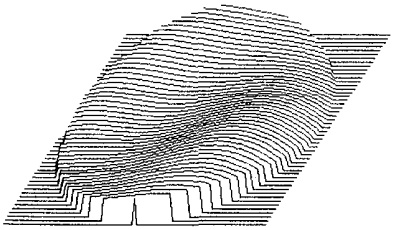

Optical surface
contour interval:0.10 λ P-V:0.55 λ RMS:0.12 λ

Figure 21. Distortion caused by the temperature pattern described in Table 2, which is the result of fitting a set of measured temperatures to the polynomial expression of equation 1. Note the change of scale.

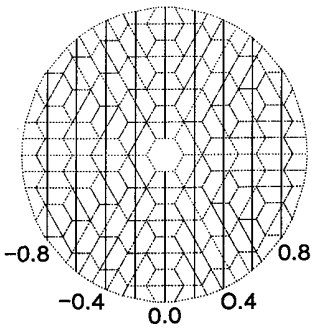

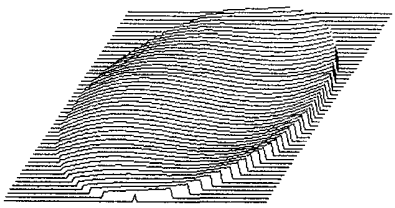

Optical surface
contour interval:0.05 λ P-V:0.117 λ RMS:0.028 λ

Figure 22. Distortion caused by a linear temperature gradient across the diameter of the mirror. This is the superposition of Figures 4 and 13. Note the change of scale.

Table 1

Summary of finite-element analysis of temperature terms from equation 1 applied to the mirror model individually.

Case	Temperature Range (°C)	Optical Surface Distortion (λ= .63 MICRONS) P-V	RMS	Focus and Tilt Removed P-V	RMS
UPPER SURFACE TEMPERATURE CASES					
K_1 = 1	+ 1-0	8.73	2.52	0.05	0.01
K_2 = 1	± 1	2.13	0.51	1.84	0.45
K_3 = 1	± 1	2.15	0.51	1.81	0.44
K_4 = 1	± 1	2.75	0.79	0.52	0.14
K_5 = 1	± 1	4.99	1.19	3.48	0.96
K_6 = 1	± 1	5.59	1.17	3.55	0.95
K_7 = 1	± 1	1.50	0.36	1.50	0.36
K_8 = 1	± 1	1.49	0.35	1.49	0.35
K_9 = 1	+ 1-.5	1.55	0.35	1.32	0.31
LOWER SURFACE TEMPERATURE CASES					
K_1 = 1	+ 1-0	9.01	2.58	0.05	0.01
K_2 = 1	± 1	2.74	0.45	1.96	0.47
K_3 = 1	± 1	2.73	0.45	1.92	0.47
K_4 = 1	± 1	1.91	0.52	0.79	0.21
K_5 = 1	± 1	3.59	0.94	2.26	0.64
K_6 = 1	± 1	4.06	0.93	2.24	0.63
K_7 = 1	± 1	0.77	0.16	0.67	0.13
K_8 = 1	± 1	0.79	0.15	0.70	0.12
K_9 = 1	+ 1-.5	1.19	0.24	0.22	0.06

Once the individual cases have been analyzed, they can be combined to produce the surface distortion from any temperature pattern expressible by the polynomial. Figure 21 is an example using measured temperature data. As described above, the measured temperatures were fit to the polynomial expression at both surfaces. The resultant polynomial coefficients are listed in Table 2. The deformations from each polynomial term can be superimposed to produce the surface shown in Figure 21.

TABLE 2

Temperature polynomial coefficients used for Figure 21 (calculated from measured data)(°C)

Mirror surface	Back surface
K_1 = .0462	K_1 = .0224
K_2 = .0242	K_2 = -.0255
K_3 = .0464	K_3 = .1095
K_4 = .0278	K_4 = -.0427
K_5 = -.0092	K_5 = .0811
K_6 = -.0536	K_6 = .0554
K_7 = -.0902	K_7 = .0488
K_8 = -.0437	K_8 = -.1195
K_9 = -.0399	K_9 = .0230

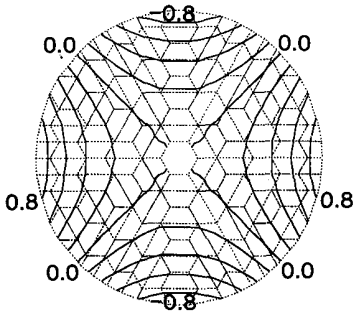

Temperature pattern
(both surfaces)

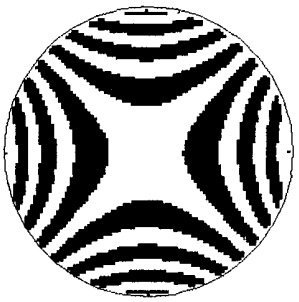

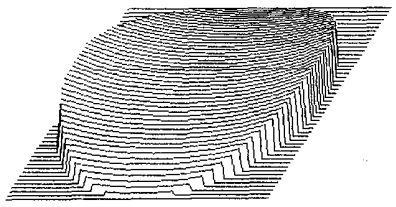

Optical surface
Contour internal 0.25λ PV:1.70λ RMS:0.33λ

Figure 23. The superposition of Figures 7 and 16. There is no temperature gradient in the axial (z) direction.

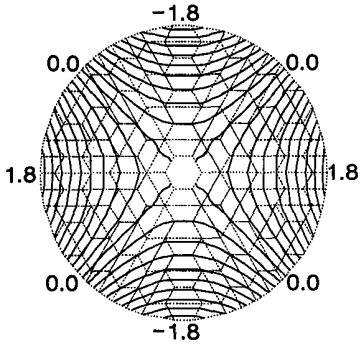

Temperature gradient
(front - back)

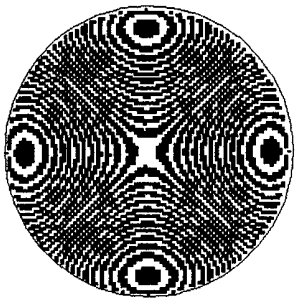

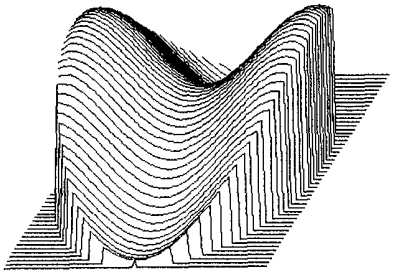

Optical surface
Contour interval:0.25λ P-V:5.78λ RMS:1.63λ

Figure 24. The superposition of Figure 7 and the negative of Figure 16. Note the first plot shows axial temperature gradient rather than temperature; the temperature range is still ±1°C.

Another combined case is shown in Figure 22; this is the result of adding Figures 4 and 13, and shows the distortion caused by a linear temperature gradient across the diameter of the mirror. This is one case which was checked against the analytical solution mentioned above. In fact, the first three terms of the analytical solution can be produced by superposition of individual cases presented here: C_0 can be produced by adding together the cases $K_1 = 1$ on upper and lower surfaces and scaling; C_1 can be produced by adding together the cases $K_2 = 1$ on upper and lower surfaces and scaling; likewise, C_3 can be produced using the cases $K_3 = 1$. It is not possible to model the fourth term of the analytical solution using a superposition of the individual cases presented here. For a mirror with flat surfaces front and back, the case $K_1 = 1$ on the upper surface represents a linear gradient in the z direction, but this is not true in general for mirrors with parabolic surfaces.

Conclusions

The primary effect of a linear diametral gradient is a tilt of the optical surface; if the tilt is removed the residual distortion is coma. The magnitude of the coma is small for gradients of a degree or less. This has application in defining the environment for testing large optics: a diametral temperature gradient has little effect on the accuracy of an optical test when the test equipment is adjusted to eliminate the relative tilt. However, as can be seen from looking at the other figures, there are patterns of temperature which could occur during an optical test that are much less benign. Testing a large mirror made of borosilicate glass, or any other material with a similar coefficient of thermal expansion, requires careful attention to the thermal environment.

Focus and tilt changes cannot always be neglected in real systems. In the optical testing of large telescope mirrors, focus and tilt terms are often removed because alignment and focusing will be accomplished in the telescope assembly operation. The thermal distortions described here, however, could be changing continuously and (unless the telescope is equipped to refocus and realign itself automatically) focus and tilt errors caused by temperature variations cannot be ignored. This is especially true of multiple-mirror telescopes, such as the NNTT, where each optical system must remain properly aligned with the others.

Figures 23 and 24 illustrate another point about the thermal distortion of large mirrors. The type of thermal distribution which causes the most distortion, even after focus and tilt have been removed, is a pattern where the z-direction gradient (through the mirror thickness) varies across the surface of the mirror. Figure 23 is the superposition of the cases in Figures 7 and 16. There is no gradient in the z-direction, and the surface distortion for a range of temperature of 2 degrees is 1.7 waves peak-to-valley after focus and tilt have been removed. This is mostly the effect of an increase in rib size with temperature. By contrast, Figure 24 is the subtraction of Figure 16 from Figure 7. In this figure, the first illustration is a plot of z-direction gradient rather than temperature. With the same temperature range of 2 degrees, the distortion after removing focus and tilt is now 5.8 waves peak-to-valley. This is because the z-direction gradient tends to cause a local curvature change, and variation of this gradient over the surface of the mirror causes a variation of curvature over the surface. By comparing these two figures, one can see that for a honeycomb-core sandwich mirror structure, this local bending can have a larger effect on the optical figure than the effects of rib growth for the same range of temperature.

One caution in using these results: in general, the surface distortions produced by a temperature pattern in this mirror will not be the same as the distortion caused by an identical pattern in a mirror with different geometry, such as a solid mirror, or one with open ribs on the back. An exception to this, however, is the analytical case described above. It was derived for and is applicable to any parabolic mirror, regardless of its structural design. This is because the assumed linear temperature distribution produces displacements but no stresses and is therefore independent of mirror structure. Other temperature distributions, in general, produce stresses which must be satisfied at all boundaries. Differences in mirror geometry will therefore change the pattern of stresses, resulting in different displacements.

References

1. Pearson, E., Stepp, L., Wong, W.-Y., Fox, J., Morse, D., Richardson, J., Eisenberg, S., "Planning the National New Technology Telescope (NNTT): III. primary optics - tests on a 1.8-m borosilicate glass honeycomb mirror." SPIE Proceedings, Vol. 628, pp. 91-101, 1986.

2. Bathe, K. J., Wilson, E. L., Peterson, F. E., "SAP IV, A structural analysis program for static and dynamic response of linear systems." University of California at Berkeley, 1974.